SCIENTIFIC REPORTS
natureresearch

OPEN

Role of S^{2-} ions on the microstructure change and the pitting behaviour of aluminum in saline solution

Received: 19 May 2019
Accepted: 30 July 2019
Published online: 19 August 2019

Mohamed M. EL-Deeb

The electrochemical behaviour and the passive film microstructure of aluminum during its exposure to 3.5 wt% NaCl solution in the absence and presence of S^{2-} ions are investigated using potentiodynamic polarization curves, electrochemical impedance spectroscopy measurements, XRD, XRF, SEM and AFM. Electrochemical measurements show that the presence of S^{2-} ions enhances the uniform corrosion of aluminum in NaCl solution, but delay its susceptibility to the pitting corrosion. In addition, EIS analysis illustrate that the formation of more compact and protective passive layer in the presence of S^{2-} ions compared to its rough surface in the absence of S^{2-} ions as evidenced by the lower value of constant phase element (*CPE*) and higher value of phase shift (*N*). Cracks, non- homogenous and open large pits with high degree of roughness are clearly observed on the aluminum surface in the absence of S^{2-} ions, compared to oriented grooves, elongated ridges with the accumulation of the corrosion products inside the pits in the presence of S^{2-} ions. The inhibitory effect of S^{2-} ions for the pitting corrosion of aluminum is interpreted on the basis of the change in its microstructure of the passive film in the absence and presence of S^{2-}ions.

Aluminum and its alloys are widely used in industrial applications, because of their good mechanical and industrial properties as well as, their highly corrosion protection[1–4]. Aluminum when immersed in chloride solutions, it will expose to the pitting corrosion, that limits its industrial and marine applications[5]. The pitting corrosion of 7A60 aluminum alloy in 3.5 wt% NaCl solution was investigated using electrochemical impedance spectroscopy, electrochemical noise, scanning electron microscopy and energy dispersive spectrometer[6]. Results revealed that the intense pitting corrosion in 7A60 aluminum alloy is explained to the presence of electrochemical active $MgZn_2$, Al_2MgCu and Mg_2Si, while the contribution of Al_7Cu_2Fe to the pitting corrosion is little. Zhang *et al.*[7] studied the relationship between the intergranular corrosion and the crystallographic pitting in AA2024-T351 aluminum alloy in 3.5 wt% NaCl solution. It was found that the intergranular corrosion occurs firstly, and the crystallographic pitting initiates from the crevice wall behind the intergranular corrosion front.

Sulphide polluted saline solutions are very aggressive medium for the corrosion of many metals, that used in many industrial installations processing sulfides. Corrosion behaviour of Cu-Al-5Ni alloy in 3.5 wt% NaCl solution containing different concentrations of sulphide ions was studied using electrochemical impedance spectroscopy measurements[8]. Data showed that, increasing the sulpide ion concentrations leads to increase the corrosion rate of this alloy that can be explained on the basis of the presence of Cu_2S that decrease the protective efficiencies of Cu_2O film. Dissolution of aluminum in 0.01 M NaOH solution as a function of sulphate, nitrate and sulphide ion concentrations was evaluated using electrochemical noise measurements[9]. It was determined that the corrosion rate of aluminum in the alkaline solution was occurred more seriousness in the presence of these additives, as concluded from the positive shift in the frequency to more highly frequency region. Sherar *et al.*[10], studied the effect of the sulphide ions on the aerobic corrosion of steel in near neutral saline solution using scanning electron microscopy, energy dispersive X-ray analysis and Raman spectroscopy. They found that the addition of the sulphide ions to the aerobically-exposed surface doubles the corrosion rate compared to its value in the sulphide free solution. Electrochemical performance of Cu, Cu-10Al-10Ni, Cp-Ti and C-steel in 3.5 wt% NaCl containing

Chemistry Department, Faculty of Science, Beni-Suef University, 62511, Beni-Suef, Egypt. Correspondence and requests for materials should be addressed to M.M.E.-D. (email: eldeebm@yahoo.com)

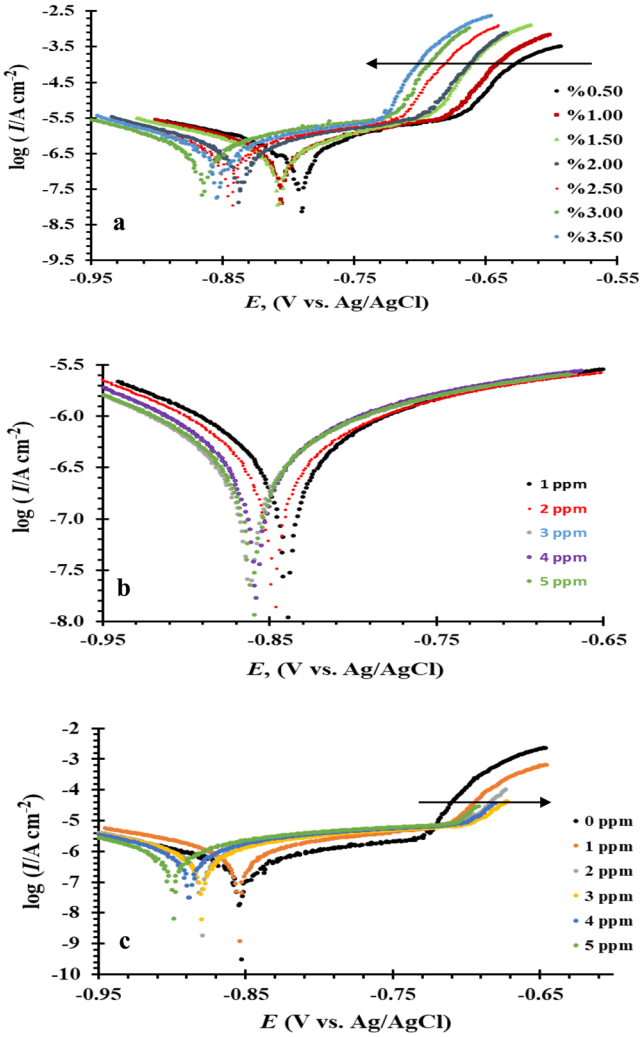

Figure 1. Potentiodynamic polarization curves of Al in (**a**) *x* wt% NaCl, (**b**) *x* ppm Na_2S and (**c**) 3.5 wt% NaCl + *x* ppm Na_2S solutions at 30 °C with scan rate of 1.0 mV s^{-1}.

C, (wt %)	E_{corr} (V vs. Ag/AgCl)	I_{corr} (μA cm^{-2})	β_a (mV dec^{-1})	β_c (mV dec^{-1})	E_{Pit} (V vs. Ag/AgCl)
0.5	−790	0.6	150.5	158	−676
1.0	−805	0.77	158.5	200	−685
1.5	−806	0.81	158.9	200	−693
2.0	−836	0.82	160.9	218	−698
2.5	−843	0.88	168.4	225	−718
3.0	−852	1.1	184.9	243	−719
3.5	−864	2.1	247.3	314	−729

Table 1. Electrochemical kinetic parameters of aluminum in *x* wt% NaCl solutions at 30 °C.

2 ppm Na_2S was studied[11]. Results clarified that the addition of S^{2-}, shifted the corrosion potential for all alloys to more negative values except Cp-Ti that be shifted to more positive.

Morphology and microstructure of the passive film play an important role for its mechanical and electrochemical properties[12]. Liu *et al.*[13] studied the effect of the abrasion on the microstructural and pitting corrosion of 2297Al-Li alloy in borate-buffered 0.001 M NaCl. Data revealed that the pitting corrosion of this alloy was strongly affected by the size, the population density and the area fraction of intermetallic particles as well as its smoother surface has lower pitting ability and better corrosion resistance compared to the rougher surface. In addition, the crystallographic orientations within a microstructure was observed to be considerable effect on pitting corrosion. It was observed the relation between the polarization and pitting behaviors with the surface orientation in pure aluminum and aluminum alloys[14–20].

Compound	Al/3.5 wt% NaCl	Al/5 ppm Na_2S	Al/3.5 wt% NaCl + 5 ppm Na_2S
Al_2O_3	99.42	99.47	99.49
MgO	0.163	0.161	0.161
Fe_2O_3	0.128	0.113	0.120
SiO_2	0.125	0.148	0.125
SO_3	0.0546	0.0476	0.0183
Na_2O	0.0389	0.0283	0.0344
Cl	0.0322	—	0.0168
TiO_2	0.0174	0.0137	0.0167
Ga_2O_3	0.0041	0.004	0.0037
CaO	0.0027	0.0021	0.0026
V_2O_5	0.0026	0.0027	0.0026
K_2O	0.0013	0.0011	—
MnO	0.0011	0.0011	—

Table 2. XRF analysis of aluminum surface immersed in 3.5 wt% NaCl, 5 ppm Na_2S and 3.5 wt% NaCl + 5 ppm Na_2S solutions for 24 hours at 30 °C.

C, ppm	E_{corr} (V vs. Ag/AgCl)	I_{corr} (μA cm^{-2})	β_a (mV dec^{-1})	β_c (mV dec^{-1})	E_{Pit} (V vs. Ag/AgCl)
1	−839	1.77	366	0.74	—
2	−846	1.92	397	0.84	—
3	−858	2.23	421	0.95	—
4	−861	2.40	506	1.08	—
5	−860	3.15	563	1.34	—

Table 3. Electrochemical kinetic parameters of aluminum in *x* ppm Na_2S solutions at 30 °C.

Effect of the microstructure on the corrosion behaviour of cast Mg-Al alloys in 5 wt. % NaCl solution saturated with $Mg(OH)_2$ was studied[21]. Data showed that the corrosion protection of homogeneous α-phase increases with increasing Al-content, due to the higher chemical stability of α-phase with higher Al contents compared to its stability with lower Al contents. The effect of heat treatment on the electrochemical corrosion and microstructural behaviour of API X70 line pipe steel in sea water containing thiosulphate solutions was evaluated[22]. Data implies that the presence of different phases of ferrite during heat treatment. Polygonal ferrite and fine grained ferrite microstructures formed at 600 °C inhibits the corrosion rate compared to the tempered martensitic microstructure formed at 300 °C. The inhibition effect was explained on to the difference in the diffusion rate of the corrosion product across the fine and coarse grained microstructure. Corrosion protection of PEO coating on extruded Al6Cu alloy in 3.5% wt NaCl was evaluated[23]. The corrosion protection of Al6Cu alloy was enhanced in the presence of PEO coating compared to as-cast alloy due to the change in its microstructure.

Yang *et al.*[24] studied the effect of sulphide ions on the passivation behaviour of titanium TA2 alloy in simulated seawater solutions. They found that the passive film was composed of TiO_2 top layer with TiO sub-oxide layer and the highly resistance of Ti substrate was correlated to the presence of TiO_2 top layer. In addition, the presence of low concentrations of highly amount of TiO_2. While at highly concentration of S^{2-} ions (>2 mM/L) decreased the corrosion resistance due to the highly fraction of TiOS and TiS_2 compared to TiO_2. The influence of sulphide ions on the passive behaviour of super 13Cr martensitic stainless steel in borate/NaCl solution was investigated[25]. Results showed that the addition of sulphide ions increased the values of the corrosion current and shifted the pitting potentials to more noble values. Moreover, the presence of sulphide ions changed the microstructure and the crystallinity of the passive layer.

By far, to our knowledge, little work reported the effect of the microstructure of the passive film on the pitting behaviour of aluminum in sulphide polluted saline solution. Therefore, the goal of our present work is to investigate the influence of the microstructure of the oxide passive film on the uniform and pitting corrosion behaviour of aluminum in 3.5 wt% NaCl solution in the absence and presence of different concentrations of Na_2S using atomic force microscopy, scanning electron microscopy, X-ray fluorescence, X-ray diffractometer, potentiodynamic polarization and electrochemical impedance spectroscopy techniques.

Experimental

Materials. Sodium chloride, sodium sulphide and acetone are provided from Merck Chemical Co. (Germany). Working electrode is made from aluminum rod with the following chemical composition (wt%): 99.57% Al, 0.31% Fe, 0.07% Si, 0.015% Ti%, 0.0016% Zn, 0.0003% Cr, 0.0019% Mg, 0.0021% Mn and 0.0007 Cu.

Microstructure characterization. The surface roughness of aluminum samples is examined using AFM measurements (Nanoscopic III E controller, Digital Instruments, Santa Barbara, CA). All AFM experiments are

C	E_{corr} (V vs. Ag/AgCl)	I_{corr} (μA cm^{-2})	β_a (mV dec^{-1})	β_c (mV dec^{-1})	E_{Pit} (V vs. Ag/AgCl)
3.5/1	−854	2.6	212	0.36	−713
3.5/2	−875	4.4	284	0.67	−705
3.5/3	−879	5.16	331	0.82	−701
3.5/4	−887	5.35	343	0.88	−698
3.5/5	−898	6.35	432	1.17	−696

Table 4. Electrochemical kinetic parameters of aluminum in 3.5 wt% NaCl + x ppm Na_2S solutions at 30 °C.

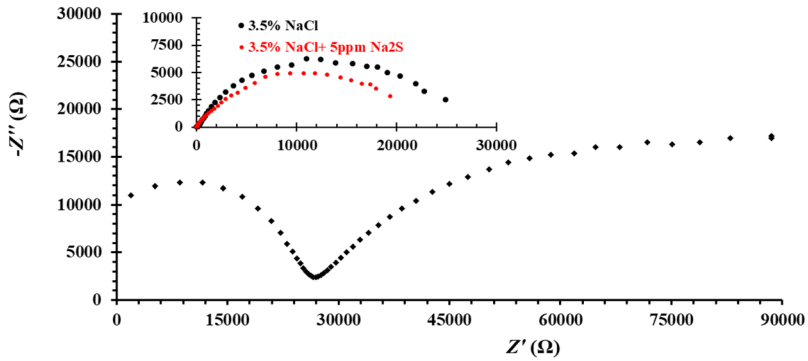

Figure 2. Nyquist plot of aluminum in 5 ppm Na_2S solution at $E_{OCP.}$ The inset represents the Nequist plots of aluminum in 3.5 wt% NaCl and in 3.5 wt% NaCl + 5 ppm Na_2S solutions at $E_{OCP.}$

performed with soft cantilevers: n^+- doped Si cantilever from Nanosensors (PPP-CONT-10), $k_n = 0.09\ N\ m^{-1}$. Scanning electron microscopy is achieved using JSM-6510LA (JEOL, Tokyo, Japan). Surface composition, crystallinity and phase identification of aluminum samples are investigated using X-ray fluorescence (ARL™ Perform'x Sequential XRF spectrometer, Thermo Scientific) and X-ray diffractometer (PANalytical Empyrean, Netherlands).

Electrochemical measurements. All the electrochemical measurements are carried out using the Potentiostat/Galvanostat (AUTOLAB PGSTAT 128 N), using a standard three-electrode cell with Al (1.0 cm^2) working, saturated Ag/AgCl reference and Pt sheet (1.0 cm^2) counter electrodes. NOVA 1.10 software is used to records and fits the electrochemical measurements. Potentiodynamic polarization measurements are achieved in the potential range between −100 to 200 mV vs. E_{OCP} values at 30 °C with the scan rate of 1.0 mV s^{-1}. Electrochemical impedance spectra at the respective E_{OCP} values are recorded using AC signals of amplitude 5 mV peak to peak in the frequency range of 10 kHz to10 MHz. Prior to each experiment, working electrode is polished successively with fine grade emery papers, cleaned with acetone, washed with bi-distilled water and finally dried.

Results and Discussion

Electrochemical measurements. *Polarization measurements.* Figure 1a represents the potentiodynamic polarization measurements of aluminum electrode in x wt% NaCl solution ($x = 0.5–3.5$), while its electrochemical parameters derived from the polarization curves (E_{corr}, E_{pit}, I_{corr}, β_a, β_c) are listed in Table 1. Results show that the presence of active/passive/pitting as the electrochemical behaviour of aluminum for all studied concentrations. It is observed that, increasing the concentrations of Cl^- ions, shifts both the corrosion potential (E_{corr}) and the pitting potential (E_{pit}) to more negative values as well as increases the values of the corrosion current densities (I_{corr}) from 0.6 μA cm^{-2} in case of 0.5 wt% NaCl solution to 2.1 μA cm^{-2} for 3.5 wt% NaCl solution. This finding explains that the rate of both uniform and pitting corrosion of aluminum increases as a results of the aggressive attack of Cl^- ions. Mechanism of the anodic and cathodic reactions associated with the uniform corrosion of aluminum in Cl^- ion solutions based on the previously reported is explained as follows[26–28]:

1 **Cathodic reaction:**

$$O_2 + 2H_2O + 2e^- \rightarrow 4OH^-{}_{(sol)} \quad (1)$$

2 **Anodic reactions:**

$$Al_{(s)} + 3e^- \rightarrow Al^{3+}{}_{(sol)} \quad (2)$$

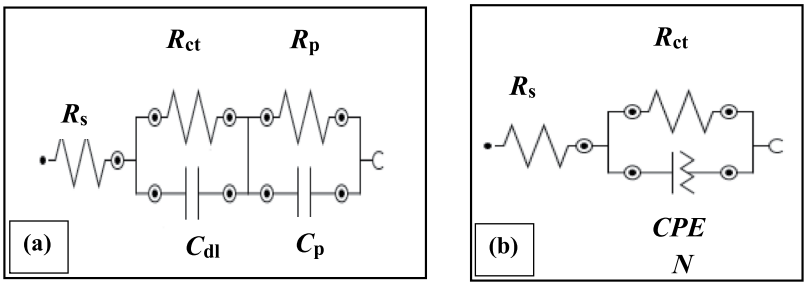

Figure 3. Electrical equivalent circuit model for aluminum/electrolyte interface in (**a**) 5 ppm Na_2S solution [R(RC)/(RC)] and (**b**) 3.5 wt% NaCl and 3.5 wt% NaCl + 5 ppm Na_2S solutions [R(RQ)].

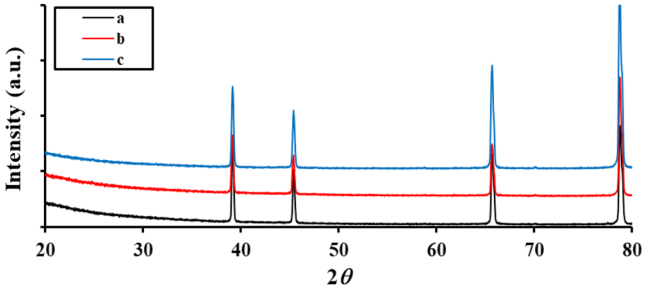

Figure 4. XRD patterns of the as-received aluminum surface immersed in (**a**) 3.5 wt% NaCl, (**b**) 5 ppm Na_2S and (**c**) 3.5 wt% NaCl + 5 ppm Na_2S solutions for 24 hours at 30 °C.

$$Al^{3+}{}_{(sol)} + 3OH^{-}_{(sol)} \rightarrow Al(OH)_{3(s)} \tag{3}$$

$$2Al(OH)_{3(s)} \rightarrow Al_2O_{3(s)} + 3H_2O \tag{4}$$

Moreover, the pitting corrosion of aluminum is explained on the basis of the reaction between the adsorbed Cl^- ions with Al^{3+} in the crystal lattice of the dual nature Al_2O_3 passive film, that consists of an adherent, compact and stable inner film covered with a porous, less stable outer film to form soluble oxychloride complex as shown in Eq. (5)[29,30].

$$Al^{3+}{}_{(crystal\ lattice)} + 2Cl^{-}{}_{(ads)} + 2OH^{-}{}_{(sol)} \rightarrow [Al(OH)_2Cl_2]^{-} \tag{5}$$

The presence of the adsorbed chloride ions on the Al_2O_3 passive film is confirmed using XRF analysis as shown in Table 2. Our results are in a good agreement with Soltis[20] and Tang *et al.*[31], who reported that the pitting potential (E_{pit}) was shifted to more negative values with increasing the concentration of the aggressive ions according to the following relation:

$$E_{pit} = A - B \log[Cl^-] \tag{6}$$

where A and B are constants, whilst A measures the aggressiveness of the chloride ions at a given concentration. Explanation of this trend can be illustrated as follows:
At low Cl^- concentration, Al^{3+} ions in the crystal lattice of the passive layer prefers to hydrolyze with OH^- rather than reacts with the Cl^- ions, therefore the growth and the propagation of the pits are decreased[27].
At high Cl^- concentration, Al^{3+} ions react with Cl^- ions producing soluble complex, that accelerates both the nucleation and the propagation of the pits[29,31].

Figure 1b represents the effect of Na_2S concentrations on the anodic and cathodic polarization curves of aluminum and the detailed electrochemical parameters are listed in Table 3. The results imply that the uniform corrosion of aluminum increases with increasing the S^{2-} ion concentrations without any sign for pitting corrosion within the studied polarization range. Mechanism of the uniform corrosion of aluminum in S^{2-} solution can be summarized as previously reported[8,32–34], S^{2-} ions is hydrogenated to give HS^-, that reacts with aluminum to produces Al_2S_3 and finally Al_2O_3 according to the following equations:

$$S^{2-} + H_2O \rightarrow HS^- + OH^- \tag{7}$$

$$Al^{3+} + HS^- + OH^- \rightarrow Al_2S_3 + H_2O \tag{8}$$

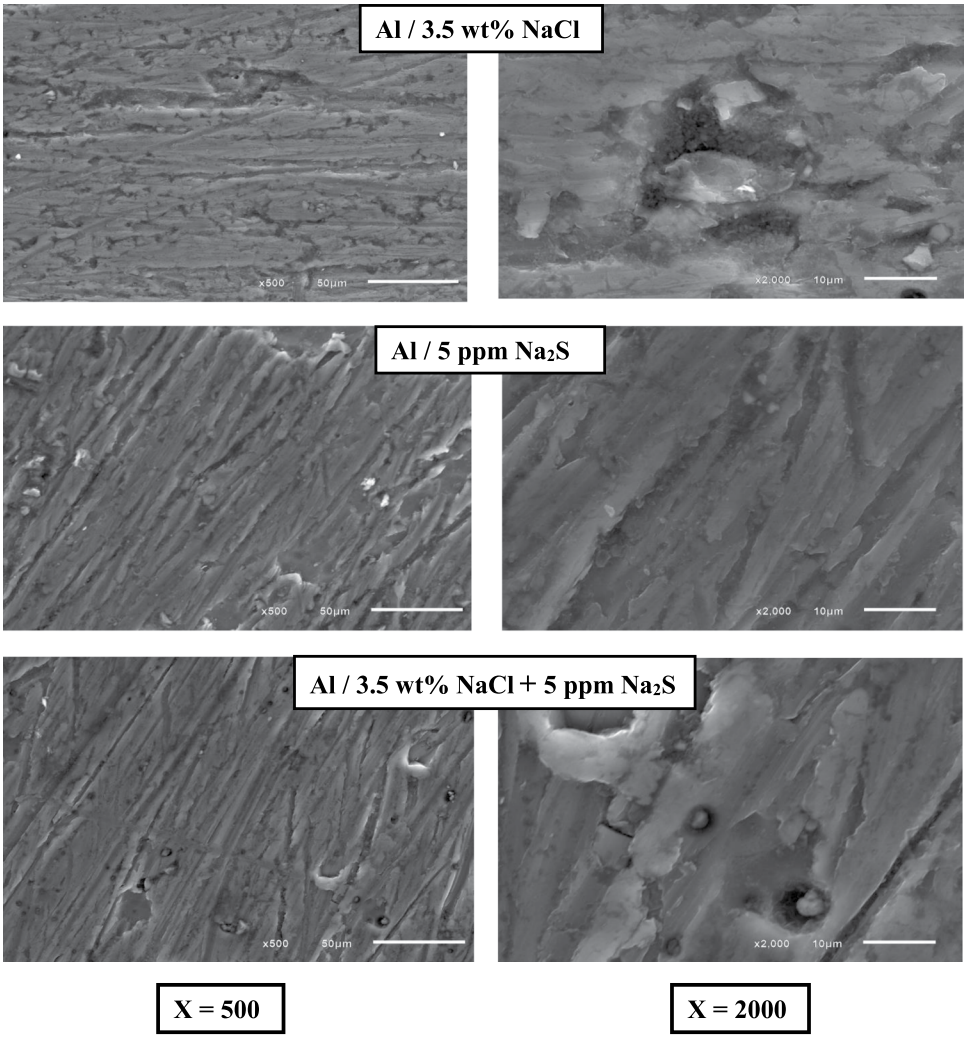

Figure 5. SEM images of the as-received aluminum surface immersed in 3.5 wt% NaCl, 5 ppm Na_2S and 3.5 wt% NaCl + 5 ppm Na_2S solutions for 24 hours at 30 °C.

$$Al_2S_3 + H_2O \rightarrow Al(OH)_3 + H_2S \tag{9}$$

$$2Al(OH)_3 \rightarrow Al_2O_3 + H_2O \tag{10}$$

The presence of Al_2O_3 as a passive film instead of Al_2S_3 is confirmed using XRF analysis (c.f. Table 2). On the other hand, the production of OH^- during the hydrogenation of S^{2-} ions as shown in Eq. (7) increases the solution pH, that explains the enhancement of the uniform corrosion rate of aluminum with increasing the concentration of S^{2-} ions.

Addition of different concentrations of Na_2S (1–5 ppm) to 3.5 wt% NaCl solution, enhances the uniform corrosion of aluminum, compared to 3.5 wt% NaCl and 5 ppm Na_2S solutions as indicated from the values of both E_{corr} and I_{corr} as shown in Tables 1, 3 and 4. In contrast, the presence of Na_2S in NaCl solution inhibits the pitting corrosion of aluminum as can be seen from Fig. 1c. The inhibition effect of S^{2-} ions on the pitting corrosion of aluminum can be seen from the decreasing in the values of the I_{pit} and increasing the difference between the values of E_{corr} and E_{pit} ($\Delta E = E_{corr} - E_{pit}$) with increasing S^{2-} ion concentrations (c.f. Fig. 1c).

Electrochemical impedance spectroscopy measurements. Electrochemical impedance spectroscopy measurements are performed to evaluate the Al/electrolyte interface with different electrolyte composition. Figure 2 represents the Nyquest plots of aluminum surface recorded at E_{OCP} in the presence of 3.5 wt% NaCl, 5 ppm Na_2S and mixture of 3.5 wt% NaCl + 5 ppm Na_2S solutions. Results point out that the presence of two consecutive capacitive semicircles in 5 ppm Na_2S solutions, that have been interpreted to the dual nature of Al_2O_3 passive film including an inner compact layer covered with outer porous layer[35]. Whereas a single semicircle is observed in both 3.5 wt% NaCl and 3.5 wt% NaCl + 5 ppm Na_2S solutions. This observation has been explained as a results of the adsorption of Cl^- ions on the Al_2O_3 passive layer, which reacts with Al^{3+} in its crystal lattice, forming soluble

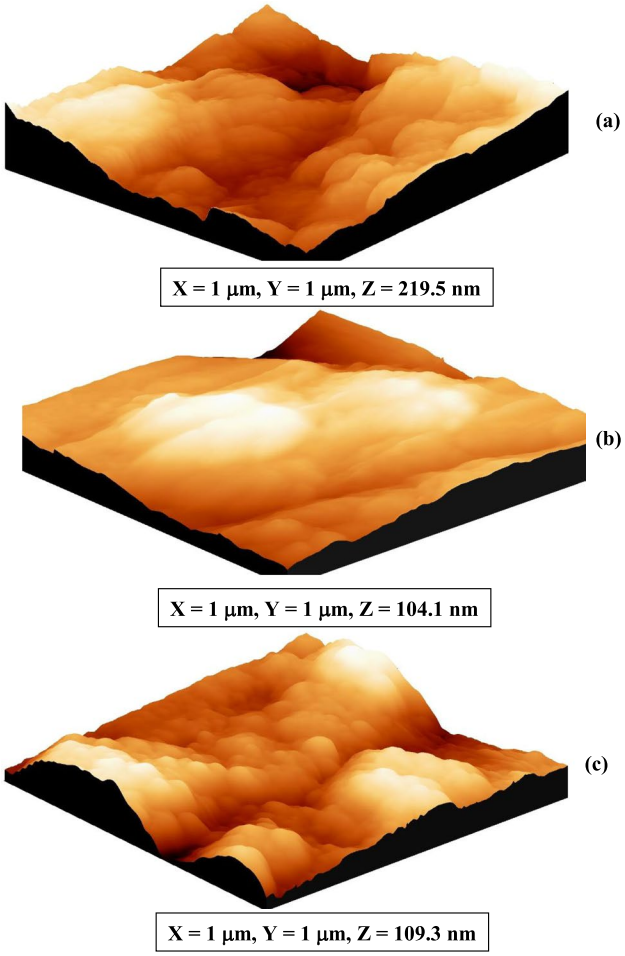

Figure 6. AFM images of the as-received aluminum surface immersed in (**a**) 3.5 wt% NaCl, (**b**) 5 ppm Na_2S and (**c**) 3.5 wt% NaCl + 5 ppm Na_2S solutions for 24 hours at 30 °C.

Sample	RMS (μm)	R_a (μm)
Al/3.5 wt% NaCl	0.355	0.343
Al/5 ppm Na_2S	0.204	0.161
Al/3.5 wt% NaCl + 5 ppm Na_2S	0.325	0.324

Table 5. AFM analysis results for aluminum surface immersed in 3.5 wt% NaCl, 5 ppm Na_2S and 3.5 wt% NaCl + 5 ppm Na2S solutions for 24 hours at 30 °C.

oxychloride complex as discussed before, leads to the dissolution of the outer porous layer. Also, the deviations of Nyquest plots in cases of 3.5 wt% NaCl and 3.5 wt% NaCl + 5 ppm Na_2S solutions from a perfect circular shape refers to frequency dispersion of interfacial impedance arising from the inhomogeneity of the electrode surface due to roughness phenomena[36]. On the other hand, the enhancement in the uniform corrosion of aluminum in 3.5 wt% NaCl + 5 ppm Na_2S solution compared to 3.5 wt% NaCl and 5 ppm Na_2S solutions is observed from the semicircle diameters as shown in the Fig. 2.

Figure 3 represents the fitted electrochemical equivalent circuit as a function in 3.5 wt% NaCl, 5 ppm Na_2S and 3.5 wt% NaCl + 5 ppm Na_2S solutions. It can be seen that the Nequest plot of aluminum in 5 ppm Na_2S solution shows [$R(RC)/(RC)$] equivalent circuit with two time constants, that agreed with the dual nature of the Al_2O_3 passive film formed in the Al/electrolyte interface. Whereas [$R(RQ)$] equivalent circuit with one-time constant is fitted to the experimental data obtained in 3.5 wt% NaCl and 3.5 wt% NaCl + 5 ppm Na_2S solutions due to the dissolution of the outer Al_2O_3 passive layer under the influence of its attack with the adsorbed Cl^- ions. Moreover, the replacement of the double layer capacitance (C_{dl}) in the [$R(RC)/(RC)$] equivalent circuit with constant phase element (CPE) and phase shift (N) in [$R(RQ)$] equivalent circuit explains the dispersion effect and the degree of heterogeneity resulted from the microscopic roughness of aluminum surface due to pitting corrosion[37–39]. The highest value of N accompanied with smallest value of CPE for aluminum in 3.5 wt% NaCl + 5 ppm Na_2S solution ($N = 0.56$ and $CPE = 54.9$ μMho) compared to their values in 3.5 wt% NaCl solution ($N = 0.52$ and $CPE = 66.1$ μMho) is calculated from the fitted experimental measurements using Boukamp model[40,41]. This means that, Al/

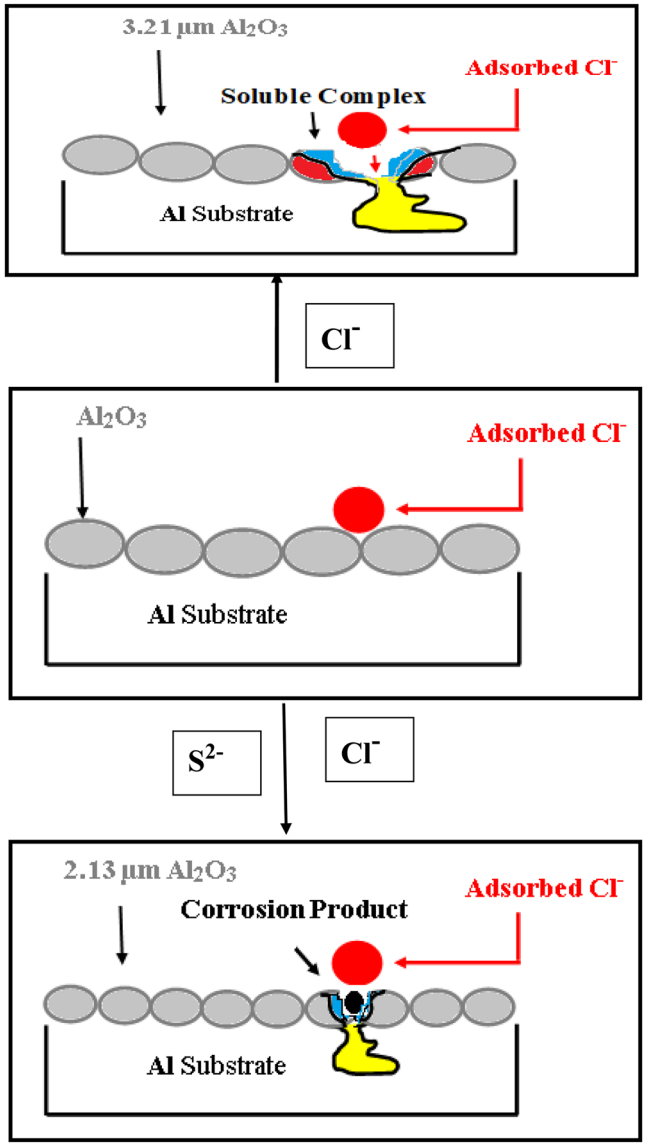

Figure 7. Schematic diagram represented the effect of S^{2-} ions on the pitting corrosion of aluminum.

electrolyte interface in 3.5 wt% NaCl + 5 ppm Na_2S solution behaves as a more ideal capacitive rather than that in 3.5 wt% NaCl, which illustrates the role of the S^{2-} ions in decreasing the roughness and increasing the homogeneity of the aluminum surface.

It is concluded from the electrochemical measurements that, even the presence of S^{2-} ions in NaCl solution enhances the uniform corrosion of aluminum but delay its susceptibility to pitting corrosion. This finding can explained on the bases of the accumulation of the corrosion products on the aluminum surface that increases the stability and the protectionist of Al_2O_3 passive layer and consequently, inhibits the rate of the pitting corrosion.

Microstructures of the aluminum surface. Figure 4 and Table 2 represents the surface composition, crystallinity and phase identification of as received aluminum surface immersed in 3.5 wt% NaCl, 5 ppm Na_2S and 3.5 wt% NaCl + 5 ppm Na_2S using X-ray fluorescence and X-Ray Diffraction analysis. Data shows that the phase composition of the passive layer is Al_2O_3 in all studied solutions, with 3.23, 0.154 and 2.127 µm average crystal size formed in 3.5 wt% NaCl, 5 ppm Na_2S and 3.5 wt% NaCl + 5 ppm Na_2S solutions respectively. SEM images for as received aluminum surface immersed in 3.5 wt% NaCl, 5 ppm Na_2S and 3.5 wt% NaCl + 5 ppm Na_2S solutions are represented in Fig. 5. Cracks, non- homogenous and open large pits with high degree of roughness are clearly observed on the aluminum surface exposed to 3.5 wt% NaCl solution in the absence of S^{2-} ions, compared to oriented grooves, elongated ridges with the accumulation of the corrosion products inside the pits in the presence of S^{2-} ions. Whilst, an intact surface with no cracks or pits are observed in case of 5 ppm Na_2S free Cl^- ions solution.

Topography of the aluminum surface immersed in 3.5 wt% NaCl, 5 ppm Na_2S and 3.5 wt% NaCl + 5 ppm Na_2S solutions is represented in Fig. 6, while its morphological parameters (*RMS* and R_a) are tabulated in Table 5. Data shows that the extensive pitting corrosion throughout the aluminum surface exposed to 3.5 wt% NaCl solution

in the absence of S^{2-} ions is indicated by the large values of both root mean square roughness (*RMS*) and average roughness (R_a) compared to their values in the presence of S^{2-} ions. This behaviour is in a good agreement with the electrochemical measurements.

The enhancement in both the roughness and the homogeneity of aluminum surface in the presence of S^{2-} ions is due to the formation of smoother, fine crystalline sized Al_2O_3 passive layer that accumulates inside the pits and inhibits their propagation, therefore decreases the susceptibility of the aluminum surface towards aggressive pitting corrosion in NaCl solution as schematically represented in Fig. 7.

Conclusion

It can be concluded that the electrochemical behaviour and the microstructure of the passive film of aluminum during its exposure to 3.5 wt% NaCl solution is strongly affected by the presence of S^{2-} ions. Increasing the concentrations of S^{2-} ions in 3.5 wt% NaCl solution increases the pH values of the saline solution, thus increasing both the anodic reaction of Al dissolution and the dissolution kinetics of Al_2O_3 passive layer resulting in an increase of the uniform corrosion. At the same time, the lower kinetic formation of smoother, compact, fine crystalline sized Al_2O_3 inhibits the pitting corrosion. The inhibitory effect is interpreted on the basis that the smooth, fine crystalline surface of Al_2O_3 increases its stability and decreases the aggressiveness of the Cl^- ions. Consequently, decreases the rate of the initiation and the growth of the stable pits.

Data Availability

The dataset generated or analyzed during the current study are available from the corresponding author upon request.

References

1. Abdallah, M., Kamar, E. M., Eid, S. & El-Etre, A. Y. Animal glue as green inhibitor for corrosion of aluminum and aluminum-silicon alloys in sodium hydroxide solutions. *J Mol Liq* **220**, 755–761 (2016).
2. Sayyah, S. M., El-Deeb, M. M., Abd El-Rehim, S. S., Ghanem, R. A. & Mohamed, S. M. Experimental and theoretical evaluation on the effect of the terminal side chain of a polymeric surfactant on the inhibition efficiency of aluminum corrosion in acid medium. *Port Electrochim Acta* **32**, 417–429 (2014).
3. Hurlen, T., Lian, H., Ogegrd, O. S. & Valand, T. V. Corrosion and passive behaviour of aluminium in weakly acid solution. *Electrochim Acta* **29**, 579–585 (1984).
4. El-Deeb, M. M., Ads, E. N. & Humaidi, J. R. Evaluation of the modified extracted lignin from wheat straw as corrosion inhibitors for aluminum in alkaline solution. *Int J Electrochem Sci* **13**, 4123–4138 (2018).
5. El-Deeb, M. M., Abdel-Shafi, N. S. & Shamroukh, A. H. Electrochemical, DFT and Mont Carlo simulations studies to evaluate the inhibition effect of novel pyridazine derivatives on iron pitting corrosion in 3.5% NaCl. *Int J Electrochem Sci* **13**, 5352–5369 (2018).
6. Wang, X.-H., Wang, J.-H. & FU, C.-W. Characterization of pitting corrosion of 7A60 aluminum alloy by EN and EIS techniques. *T Nonferr Metal Soc* **24**, 3907–3916 (2014).
7. Zhang, X., Zhou, X., Hashimoto, T. & Liu, B. Localized corrosion in AA2024-T351 aluminum alloy: Transition from intergranular corrosion to crystallographic pitting. *Mater Charact* **130**, 230–236 (2017).
8. El-Sayed, N. H. & El-Rabiei, M. M. Effect of sulphide pollution on the stability of Cu-Al-5Ni alloy in 3.5% NaCl solution. Egypt. *J Petrol* **23**, 163–168 (2014).
9. Na, K.-H. & Pyun, S.-I. Electrochemical noise analysis of corrosion of pure aluminum in alkaline solution in the presence of SO_4^{2-} ion, NO_3^- ion and Na_2S additives. *Electrochim Acta* **52**, 4363–4373 (2007).
10. Sherar, B. W., Keech, P. G. & Shoesmith, D. W. The effect of sulphide on the aerobic corrosion of carbon steel in near-neutral pH saline solution. *Corros Sci* **66**, 256–262 (2013).
11. Nady, H., El-Rabiei, M. M. & Samy, M. Corrosion behaviour and electrochemical properties of carbon steel, commercial pure titanium, copper and copper-aluminum-nickel alloy in 3.5% sodium chloride containing sulphide ions. *Egypt J Petrol* **26**, 79–94 (2017).
12. Guo, Q., Liu, J., Yu, M. & Li, S. Effect of passive film on mechanical properties of martensitic stainless steel 15-5PH in a neutral NaCl solution. *Appl Surf Sci* **327**, 313–320 (2015).
13. Liu, J., Zhao, K., Yu, M. & Li, S. Effect of surface abrasion on pitting corrosion of Al-Li alloy. *Corros Sci* **138**, 75–84 (2018).
14. Brewick, P. T. *et al.* Microstructure-sensitive modeling of pitting corrosion: Effect of the crystallographic orientation. *Corros Sci* **129**, 54–69 (2017).
15. Yasuda, M., Weinberg, F. & Tromans, D. Pitting corrosion of Al and Al-Cu single crystals. *J Electrochem Soc* **137**, 3708–3715 (1990).
16. Treacy, G. M. & Breslin, C. B. Electrochemical studies on single-crystal aluminum surfaces. *Electrochim Acta* **43**, 1715–1720 (1998).
17. Davis, B. W., Moran, P. J. & Natishan, P. M. Metastable pitting behavior of aluminum single crystals. *Corros Sci* **42**, 2187–2192 (2000).
18. Seo, J. H., Ryu, J. H. & Lee, D. N. Formation of crystallographic etch pits during AC etching of aluminum. *J. Electrochem Soc* **150**, B433–B438 (2003).
19. Koroleva, E. V., Thompson, G. E., Skeldon, P. & Noble, B. Crystallographic dissolution of high purity aluminum. *Proceedings of the Royal Society A: Mathematical, Physical and Engineering Sciences*., https://doi.org/10.1098/rspa.2007.1846 (2007).
20. Soltis, J. Passivity breakdown, pit initiation and propagation of pits in metallic materials Review. *Corros Sci* **90**, 5–22 (2015).
21. Michael, G., Andreas, L., Robert, S. & Sannakaisa, V. Influence of the microstructure on the corrosion behaviour of cast Mg-Al alloys. *Corros Sci* **155**, 195–208 (2019).
22. Sharm, L. & Chhibber, R. Microstructure evolution and electrochemical corrosion behaviour of API X70 linepipe steel in different environments. *Int J Pres Vis Pip* **171**, 51–59 (2019).
23. Zhu, L. *et al.* Microstructure and corrosion resistance of the PEO coating on extruded Al6Cu alloy. *Surf Coat Technol* **369**, 116–126 (2019).
24. Yang, X., Du, C., Wan, H., Liu, Z. & Li, X. Influence of sulphides on the passivation behaviour of titanium alloy TA2 in simulated seawater environments. *Appl Surf Sci* **458**, 198–209 (2018).
25. Lei, X. *et al.* Passivity of martensitic stainless steel in borate buffer solution: Influence of sulphide ion. *Appl Surf Sci* **478**, 225–265 (2019).
26. Amin, M. A. A newly synthesized glycine derivative to control uniform and pitting corrosion processes of Al induced by SCN^- anions – Chemical, electrochemical and morphological studies. *Corros Sci* **52**, 3243–3257 (2010).
27. Zhang, K. *et al.* Inhibitory effect of konjac glucomanan on pitting corrosion of AA5052 aluminum alloy in NaCl solution. *J Colloid Interf Sci* **517**, 52–60 (2018).
28. Wang, D. *et al.* Electrochemical and DFT studies of quinoline derivatives on corrosion inhibition of AA5052 aluminum alloy in NaCl solution. *Appl Surf Sci* **357**, 2176–2138. (2015).

29. Sherif, E., El-Danaf, E., Soliman, M. & Almajid, A. Corrosion passivation in natural seawater of aluminum alloy 1050 processed by equal-channel-angular-press. *Int J Electrochem Sci* **7**, 2846–2859 (2012).
30. Brett, C., Gomes, I. & Martins, J. The electrochemical behaviour and corrosion of aluminum in chloride media. *The effect of inhibitor anion. Corros Sci* **36**, 915–923 (1994).
31. Tang, Y. *et al*. The metastable pitting potential and its relation to the pitting potential for four materials in chloride solutions. *Corros Sci* **80**, 111–116. (2014).
32. Guan, F. *et al*. Influence of sulfate-reducing bacteria on the corrosion behavior of 5052 aluminum alloy. *Surf Coat Technol* **316**, 171–179 (2017).
33. Rockel, M. B., Schedlitzky, D. & Bender, R. Aluminum alloys, Corrosion Handbook. *Wiley-VCH Vertag GmbH&Co. KGaA* (2008).
34. Wiberg, N. & Holleman, A. F. Inorganic Chemistry. Academic Press: San Diego (2001).
35. Datta, J. *et al*. Role of Cl^- and NO_3^- ions on the corrosion behaviour of 20% SiCp reinforced 6061-Al metal matrix composite: A correlation between electrochemical studies and atomic force microscopy. *Corros Sci* **50**, 2658–2668 (2008).
36. Bouyanzer, A., Hammouti, B. & Majidi, L. Pennyroyal oil from Mentha pulegium as corrosion inhibitor for steel in 1 M HCl. *Mat Lett* **60**, 2840–2843 (2006).
37. Jüttner, K. Electrochemical impedance spectroscopy (EIS) of corrosion processes on inhomogeneous surfaces. *Electrochim Acta* **35**, 1501–1508 (1990).
38. Peng, G. S., Chen, K. H., Fang, H. C., Chao, H. & Chen, S. Y. EIS study on pitting corrosion of 7150 aluminum alloy in sodium chloride and hydrochloric acid solution. *Mater Corros* **61**, 783–789 (2010).
39. Cao, C & Zhang, J. Electrochemical impedance spectroscopy introduction. Science Press, Beijing (2002).
40. Boukamp, B. A. A nonlinear least squares fit procedure for analysis of immittance data of electrochemical systems. *Solid State Ionics* **20**, 31–44 (1986).
41. El-Deeb, M. M., Alshammari, H. M. & Abdel-Azeim, S. Effect of ortho-substituted aniline on the corrosion protection of aluminum in 2 mol/L H_2SO_4 solution. *Can J Chem* **95**, 612–619 (2017).

Additional Information

Competing Interests: The authors declare no competing interests.

Publisher's note: Springer Nature remains neutral with regard to jurisdictional claims in published maps and institutional affiliations.

Open Access This article is licensed under a Creative Commons Attribution 4.0 International License, which permits use, sharing, adaptation, distribution and reproduction in any medium or format, as long as you give appropriate credit to the original author(s) and the source, provide a link to the Creative Commons license, and indicate if changes were made. The images or other third party material in this article are included in the article's Creative Commons license, unless indicated otherwise in a credit line to the material. If material is not included in the article's Creative Commons license and your intended use is not permitted by statutory regulation or exceeds the permitted use, you will need to obtain permission directly from the copyright holder. To view a copy of this license, visit http://creativecommons.org/licenses/by/4.0/.

© The Author(s) 2019